nature physics

ARTICLES

PUBLISHED ONLINE: 17 OCTOBER 2010 | DOI: 10.1038/NPHYS1794

Real-space observation of emergent magnetic monopoles and associated Dirac strings in artificial kagome spin ice

Elena Mengotti[1], Laura J. Heyderman[1]*, Arantxa Fraile Rodríguez[1†], Frithjof Nolting[1], Remo V. Hügli[2] and Hans-Benjamin Braun[2]*

Magnetic monopoles have been predicted to occur as emergent fractional quasiparticles inside pyrochlore spin ice, a frustrated magnetic insulator. Experimental signatures of such emergent monopoles accompanied by Dirac strings have been detected by means of neutron scattering in reciprocal space in pyrochlore spin ice at sub-Kelvin temperatures, but their real-space observation has remained elusive. Here we report on direct, real-space observations of emergent monopoles and their associated Dirac strings in two-dimensional (2D) artificial kagome spin ice at room temperature using synchrotron X-ray photoemission electron microscopy. Magnetization reversal proceeds through the nucleation and avalanche-type dissociation of monopole–antimonopole pairs along 1D Dirac strings. This is in sharp contrast to conventional domain growth in 2D systems, providing a striking example of dimensional reduction due to frustration. The observed hysteresis, monopole densities and 1D Dirac-string avalanches are quantitatively explained by Monte Carlo simulations.

Magnetic monopoles have inspired the imagination of physicists ever since Dirac's observation that their existence can be reconciled with quantum mechanics[1]. These Dirac monopoles reside at the ends of an infinitesimal flux tube corresponding to a singularity of the vector potential, the so-called Dirac string. Monopoles without such string-like singularities may exist when the gauge group of electromagnetism is embedded in higher symmetry non-Abelian gauge groups[2,3], and correspondingly elementary monopoles are predicted by grand unified theories and by supersymmetric generalizations of the standard model of particle physics. Observation of elementary monopoles would thus lend support to models that go beyond the standard model but, despite an intense search[4,5], such monopoles have not been found so far.

Here we follow a different, more modest approach and investigate emergent monopoles in a condensed-matter setting, which share similarities with the monopoles conceived by Dirac. Such monopoles have been predicted to occur as fractional quasiparticles inside pyrochlore spin ice[6]. These systems are characterized by so-called ice rules, where, in the tetrahedral coordination of the pyrochlore structure, two of the four Ising type spins on the vertices point towards the tetrahedral centre whereas the other two spins point away[7–9], reminiscent of proton ordering in water ice[10]. The emergence of magnetic monopoles is most clearly seen within a charge model[6], where the spin magnetic moment is considered to be stretched into a charge dumbbell with the charges $\pm q$ residing at the centres of neighbouring tetrahedra that form a diamond lattice. The ice-rule ground state is then characterized by zero net charge at each diamond-lattice site. Overturning a dipole leads to non-zero and opposite charges $\Delta Q = \pm 2q$ at the centres of neighbouring tetrahedra. As a result of the pyrochlore structure, these charges can easily be separated by flipping adjacent dipoles along a 1D path on which the ice rule is maintained, and non-zero charges reside only at its ends. If these charges separate, they may be regarded as independent monopoles (antimonopoles), their signature being a non-zero value of a 'smeared' or 'coarse-grained' charge density[6] ρ_m averaged over distances larger than the lattice constant. The decay of a dipolar excitation into constituent monopoles provides an example of fractionalization in three dimensions[6,11,12]. Such a phenomenon is well known in both one dimension, for example as charge solitons in polyacetylene[13], or the decay of magnons into spinons in spin chains[14–16], and in two dimensions, as fractionally charged excitations in the quantum Hall effect[17,18].

In pyrochlore spin ice, the monopole–antimonopole pairs are connected by a string of overturned dipoles, which is often called a Dirac string[6,19–21]. In this context, the Dirac string is understood as a physical 1D object that feeds magnetic flux into the volume elements where the monopoles reside. The string was originally conceived by Dirac as a singular line in the vector potential, to describe the quantum motion of an electron in the (classical) field of a magnetic monopole. Invoking the single-valuedness of the electronic wavefunction, Dirac inferred that the string must carry an integer multiple of the flux quantum, implying the famous quantization of the monopole strength[1]. It should be emphasized, however, that although 'invisible' to electrons surrounding them, such strings carrying one (Cooper pair) flux quantum are not invisible per se in a condensed-matter setting. They may very well be observed, for example as flux lines in superconductors by means of neutron scattering[22,23], and the absence of their termination in the bulk is aptly referred to as the 'no-monopole condition'[24]. Reciprocal space signatures of such Dirac strings and associated monopoles have recently been detected in the

[1]Paul Scherrer Institute, 5232 Villigen PSI, Switzerland, [2]School of Physics, University College Dublin, Dublin 4, Ireland. †Present address: Departament de Física Fonamental and Institut de Nanociència i Nanotecnologia (IN2UB), Universitat de Barcelona, 08028 Barcelona, Spain.
*e-mail: laura.heyderman@psi.ch; beni.braun@ucd.ie.

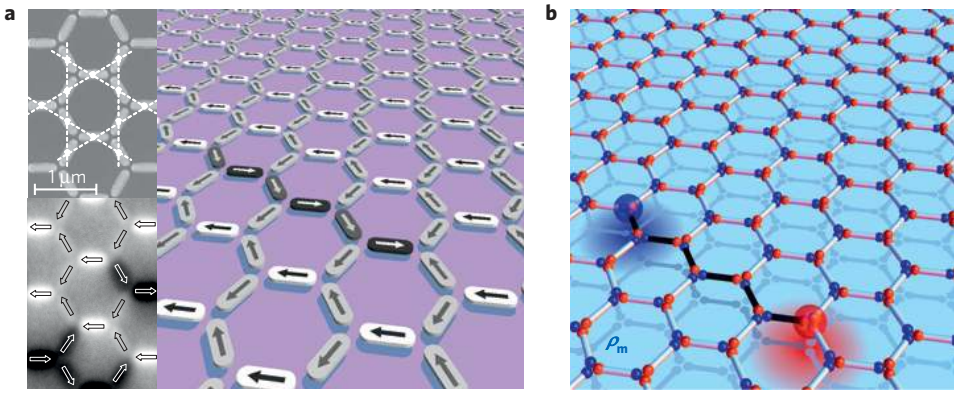

Figure 1 | Emergent monopoles and associated Dirac strings in artificial kagome spin ice. a, Schematic view of the nanolithographic array of permalloy islands with anisotropy axes along honeycomb links and the orientation of the magnetization indicated by arrows. Initially, the sample is magnetized to the left and applying a reversed field induces the formation of a Dirac string with two monopole defects residing at its ends. The island colour corresponds to the contrast in the XMCD image, which is a measure of the orientation of the magnetization (see Methods, Experiment). Inset: Scanning electron microscope image of part of the sample, with the kagome lattice overlaid, together with an example of a corresponding XMCD image; the uniform contrast associated with each island confirms that they are monodomain and unambiguously determines the orientation of the magnetization pointing along each island. **b**, Corresponding charge distribution with magnetic moments replaced by dumbbells carrying charge q and $-q$ (in red and blue). At each vertex, three charges coalesce, and the saturated state with moments pointing towards the left is characterized by an alternating NaCl-type charge ordering. Along the Dirac string (dark contrast), the charge dumbbells are overturned, resulting in two charge defects with charges $\Delta Q = \pm 2q$ at the ends of the string as indicated by the large spheres. Background plane (in light blue): the two charge defects manifest themselves as distinct peaks in the smeared charge density ρ_m which characterizes the two defects as a well-separated monopole–antimonopole pair.

	I. Initial state	II. Mobile monopole (MP)		III. Vertex on a Dirac string	IV. Not observed	V. Trapped MP
Moments						
Dumbbell						
Q_α	$-q$	$+q$	$-3q$	$-q$	$+3q$	$+q$
ΔQ_α	0	$+2q$	$-2q$	0	$+4q$	$+2q$
Moments						
Dumbbell						
Q_α	$+q$	$-q$	$+3q$	$+q$	$-3q$	$-q$
ΔQ_α	0	$-2q$	$+2q$	0	$-4q$	$-2q$

Figure 2 | Identification of monopoles during magnetization reversal. Schematic overview of all vertex configurations, the corresponding dumbbell representation and their association with monopole defects. The grey scale used for the islands indicates the corresponding XMCD contrast. The total charge Q_α is shown for each vertex configuration, together with the charge difference $\Delta Q_\alpha = Q_\alpha - Q_{0,\alpha}$ relative to the initial charge configuration $Q_{0,\alpha}$, which is realized here by the initial saturated state where all moments point towards the left (column I). On application of a reverse magnetic field, individual moments will reverse, as highlighted in yellow. A mobile monopole exists when one moment around a vertex is reversed (column II). When two head-to-tail magnetic moments are reversed, the total magnetic charge associated with the vertex does not change ($\Delta Q_\alpha = 0$) and a configuration encountered in the interior of a Dirac string is obtained (column III). The reversal of two head-to-head (tail-to-tail) moments shown in column IV is never observed, as explained by the charge model (see Methods, Theory). Column V shows a state with all moments reversed. This state describes a charge defect that sits on a Dirac string and is trapped, that is, it can no longer move on further increase of the applied field.

pyrochlore systems[20,21,25] $Ho_2Ti_2O_7$ and $Dy_2Ti_2O_7$ at sub-Kelvin temperatures, and monopole-type defects have been reported in artificially produced connected honeycomb networks[26]. However, a direct, real-space observation of the interplay of Dirac strings and monopoles has not been reported to date.

In this work, we directly observe monopoles and the associated Dirac strings in artificial kagome spin ice at room temperature, and we demonstrate that magnetization reversal occurs by means of the creation and separation of emergent monopole–antimonopole pairs, leaving such a Dirac string of overturned dipoles in their wake. Our results open the way to manipulate magnetic charges in the same fashion as electric charges, a concept that could lead to new types of logic and spintronic device.

Monopoles and Dirac strings in artificial spin ice

An elegant way to directly visualize monopole-type defects and Dirac strings at room temperature is to study an artificial frustrated system, namely an array of lithographically fabricated isolated single-domain nanomagnets. In such a system, the dipolar interactions create a 2D analogue of pyrochlore spin ice[27] and the moment configurations can be observed directly by employing various magnetic microscopy methods[27–29]. As nanomagnets arranged on the links of a square lattice require inequivalent heights to demonstrate strict spin ice behaviour, we choose to study an artificial kagome spin ice with the nanomagnets centred on the sites of a kagome lattice (Fig. 1a), where no height offset is necessary[30]. Here, the nanomagnets form the links of a honeycomb lattice and the ice rules now dictate a two-out/one-in or two-in/one-out configuration on a vertex of the honeycomb lattice[31]. Such a kagome spin ice phase also arises when a 3D pyrochlore spin ice is exposed to a magnetic field along the [111] direction[32,33].

In close analogy to the 3D pyrochlore spin ice, the charge model is obtained by stretching each dipole with magnetic moment m into a dumbbell with two opposite magnetic charges of magnitude $q = m/a_h$ located at its ends at the two neighbouring vertices of the honeycomb lattice, separated by a_h (see Fig. 1). At each vertex α, three charges coalesce, enforcing a non-vanishing vertex charge $Q_\alpha = \sum_{n\in\alpha} q_n$ that is composed of the individual charges $q_n = \pm q$. The charge model (see Methods) then predicts an NaCl-type charge-ordered ground state that is twofold degenerate with respect to the sublattice parity in the absence of an external magnetic field[34,35] as it minimizes both the intrasite and intersite Coulomb interaction. Note, however, that this ground state of the charge model may also be realized by magnetically disordered states[35]. For these ground states, the 'smeared' or 'coarse-grained' charge density ρ_m becomes exponentially small when averaging is carried out over distances larger than a_h. Such a coarse-grained charge density would describe, for example, the response of a low-resolution magnetic force microscope (MFM)-type measurement. Within a coarse-grained charge description (see Fig. 1b), our system is equivalent to the 3D pyrochlore system.

Charge excitations and monopoles in the artificial kagome ice are now created analogous to 3D pyrochlore spin ice. For definiteness, we consider the experimentally relevant situation where the system is initially set in an external magnetic field. This initial saturated state constitutes one particular realization of the charge model ground states. We now follow a strategy that is related to that pursued by Morris *et al.* in their studies of 3D pyrochlore spin ice[20]. On applying a reversed field, the flipping of a single dipole leads to an inversion of a charge dumbbell and induces an incipient monopole–antimonopole pair at two neighbouring sites. The monopole or antimonopole corresponds to an excess charge $\Delta Q_\alpha = Q_\alpha - Q_{0,\alpha} = 2q$ or $-2q$, respectively, above the charge configuration $Q_{0,\alpha}$ of the initial state. This initial state is shown in Fig. 2, column I, and is also the state surrounding the Dirac string in Fig. 1b. As illustrated in Fig. 1, the monopole–antimonopole pair

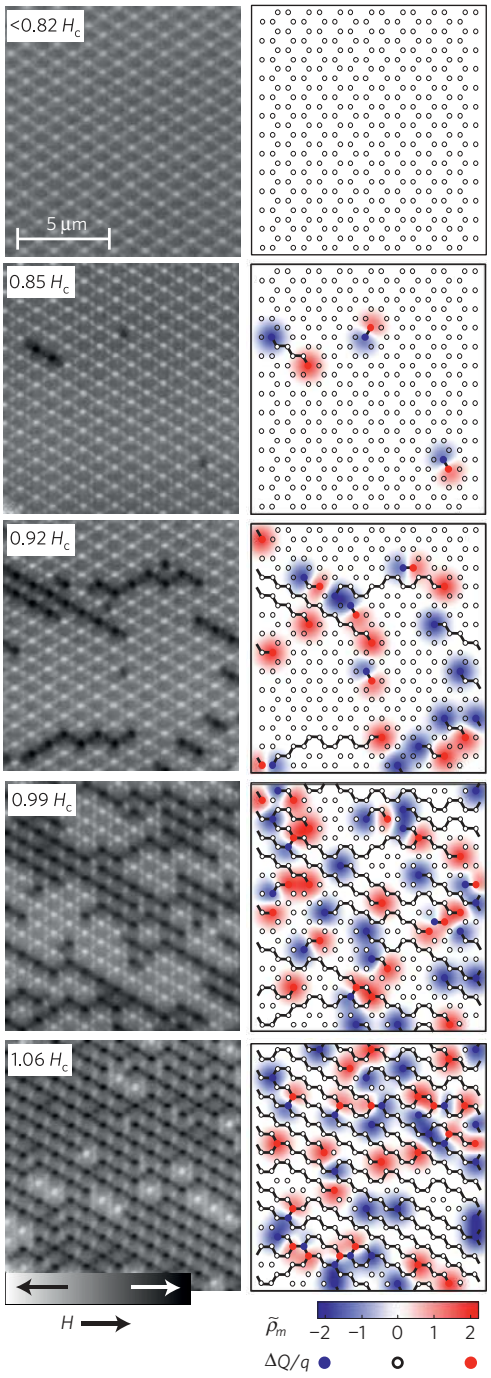

Figure 3 | Creation and separation of monopole–antimonopole pairs and growth of Dirac strings. XMCD images (left panels) together with the associated ΔQ map (right panels), in the initial saturated state and at four evenly spaced field values. The initial configuration has all moments pointing towards the left (bright XMCD contrast) and exhibits no charge defects ($\Delta Q = 0$) as indicated by white dots in the schematics. On applying a magnetic field to the right, the island moments switch, with the XMCD contrast changing from bright to dark, and monopole–antimonopole pairs ($\Delta Q = +2q$ and $-2q$ indicated with red and blue dots) are created and separate. The history of the propagation of monopole–antimonopole pairs is delineated by Dirac strings consisting of chains of dark islands with reversed moments shown as a continuous line in the schematics. The ΔQ map is shown together with the dimensionless coarse-grained magnetic charge density $\tilde{\rho}_m$ (see Methods). Note the excellent agreement between the ΔQ and $\tilde{\rho}_m$ maps, which both serve as signatures for non-vanishing monopole density in this field regime.

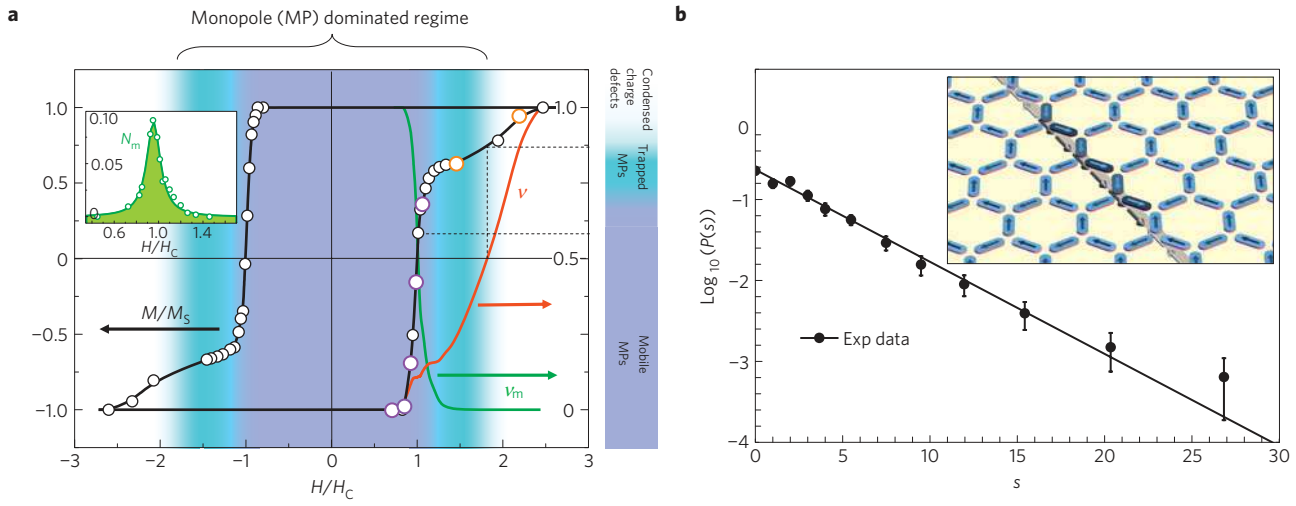

Figure 4 | Hysteresis and avalanches—experimental results. a, Hysteresis (black), charge defect density ν (red) and fraction of mobile monopoles ν_m (green). Purple circles indicate field values where the images of Fig. 3 are taken, and the orange circles indicate the high field data shown in Supplementary Fig. S2. During the onset of the hysteresis, incipient monopole–antimonopole pairs are created. Subsequently these mobile pairs dissociate and the monopole density shows a small plateau in the red curve. Towards the end of the initial steep rise of the hysteresis, many Dirac strings extend over large distances, making it likely that monopoles get trapped at neighbouring strings, leading to the loss of mobile monopoles (see last panel in Fig. 3). The plateau is characterized by a stripe phase of Dirac strings (see top panels of Supplementary Fig. S2), leaving most moments in the one-island bridges between strings unflipped. Inset: Number of mobile monopoles per site, N_m, as a function of applied field. Mobile monopoles occur predominantly within the sharp rise of the hysteresis. **b**, The probability $P(s)$ to encounter a Dirac string avalanche of length s decays exponentially, similar to the 1D RFIM (ref. 40), providing a demonstration of the 1D nature of the Dirac string avalanches. The avalanche statistics have been obtained by summing over all avalanches occurring between the consecutive non-zero field values shown in Fig. 3. Error bars are statistical, derived from the square root of the number of events. Inset: Formation of Dirac string avalanches is an example of dimensional reduction due to frustration. Shown is a Dirac string configuration with a schematic of the Ising pseudospin directions illustrating the close analogy between emergent fractionalized monopoles and 1D fractionalization due to solitons[14–16].

can be separated further by flipping dipoles along a continuous path leaving a Dirac string of overturned dipoles between them, which does not alter the original charge order (Fig. 2, column III) except at the positions where the monopole or antimonopole reside. When a monopole of a given charge, say $\Delta Q = +2q$, sweeps across the sample, it passes sites with charge $\pm q$, thus raising the local charge to either $+3q$ or $+q$, depending on the sublattice. It should be pointed out that these charge defects in general give rise to non-vanishing ρ_m (see Fig. 3), confirming that they may be regarded as emergent monopoles.

At fields smaller than the coercivity H_c and in a field range extending over more than half the hysteresis loop, the behaviour of artificial spin ice closely resembles that of 3D pyrochlore spin ice. The charge defects defined with respect to the initial saturated state are mobile (see Fig. 2, column II) and, as they give rise to non-vanishing ρ_m, they can be considered as free emergent monopoles, see Fig. 1b. At higher fields the differences from the pyrochlore spin ice become apparent: for $H > H_c$, the monopoles, as well as generally still leading to non-zero ρ_m, become increasingly trapped on the ever-proliferating Dirac strings (see Fig. 2, column V). This trapping of monopoles may provide the exciting possibility for the controlled manipulation of charge defects (see Supplementary Fig. S1). Only in the very last stages of the magnetization reversal do the charge defects actually 'condense' into the time-reversed state of the initial state, which has again zero smeared charge density ρ_m. Monopole-type defects in this regime should then be described as charge defects with respect to the time-reversed state (see Supplementary Fig. S2).

Visualization of monopoles and Dirac strings

Experimentally, we have realized an artificial kagome spin ice, comprising quasi-infinite nanolithographic arrays of individual elongated permalloy islands[28], providing an analogue of the spins in the pyrochlore compounds. With photoemission electron microscopy, we were able to directly follow the creation and separation of monopole–antimonopole pairs in real space and image the Dirac string of overturned dipoles that are left in their wake (see schematic in Fig. 1a). The single contrast associated with each island in the X-ray magnetic circular dichroism (XMCD) images (see Fig. 1a inset and Fig. 3) indicates that they are monodomain and therefore mesoscopic analogues of Ising spins, with the shape anisotropy playing the role of the Ising anisotropy.

We begin by applying a saturating magnetic field such that, after its removal, all moments point towards the left (Fig. 3, panel 1). As was illustrated in Fig. 1, monopoles and Dirac strings are now created by applying a field in the reversed direction. Each field step triggers the growth of the Dirac strings in the form of a 1D avalanche, with several adjacent dipoles flipped until the avalanche comes to a rest, as illustrated by Fig. 3, panels 2–5. Note that in contrast to the pyrochlore spin ice[6,20,21], where the monopoles form a gas and the Dirac strings are dynamically fluctuating, in this artificial spin ice system the shape anisotropy associated with each magnetic island has an energy of the order of 10^4 K. We are thus effectively dealing with a low-temperature situation where, after each field step, disorder in the form of random variations in the switching field leads to pinning of the monopoles and hence of the Dirac strings connecting them. This permits imaging of the dipole configurations at zero field before increasing the field to a higher value.

The schematics associated with the XMCD snapshots in Fig. 3 highlight the position of the monopoles (antimonopoles) with red (blue) dots, corresponding to $\Delta Q/q = +2$ (-2). In the XMCD images, islands in the initial state (moments pointing towards the left) have a bright contrast and islands where the moments have reversed to the right have a dark contrast (see also Figs 1

and 2). A closer inspection of Fig. 3 reveals that magnetization reversal starts with the flipping of individual islands creating a monopole–antimonopole pair at the neighbouring vertices. These islands are characterized by low values of the randomly modulated switching field, which can be controlled for individual islands as demonstrated in the Supplementary Fig. S1. After creation, these monopole–antimonopole pairs separate and their path, that is, the history of their displacement, is imprinted as a dark chain of islands with reverse moments, which corresponds to a physical version of a Dirac string[6] and is indicated by a continuous line in the schematics of Fig. 3. The Dirac strings grow horizontally or diagonally as a result of 1D avalanches. Here, the monopoles always propagate to the right and the antimonopoles to the left, being attracted to the applied field poles of opposite sign. It should be noted that we never observe, either in experiments or in simulations, defects with $\Delta Q = \pm 4q$ (see Fig. 2, column IV), a fact that can be explained by the charge model (see Methods, Theory).

From the XMCD images we can directly determine the hysteresis curve $M(H)$, the number of mobile and trapped monopoles, and avalanche statistics, as shown in Fig. 4a,b. The analysis has been carried out on a 25 μm × 30 μm area containing 2,550 islands. Three distinct regimes of the hysteresis may be discerned: a steep rise, followed by a plateau-like feature and a final slow saturation towards the completely reversed state. The initial part of the hysteresis is characterized by the nucleation of incipient monopole–antimonopole pairs, with a concomitant rise in the charge defect density, ν. Following nucleation, these monopole–antimonopole pairs dissociate and expand the Dirac string in an avalanche-type fashion, causing a sharp increase of the magnetization, while remarkably, the monopole density shows a plateau, remaining at a small value. This regime persists up to field values above the coercivity H_c, and hence over more than half the hysteresis loop. Slightly above H_c, the increasing number of Dirac strings makes it likely that mobile monopoles hit another Dirac string and thus become trapped. This is evidenced by the sharp drop in the number of mobile monopoles in this regime (see inset in Fig. 4a). The plateau in the hysteresis corresponds to a stripe phase of Dirac strings where one of the three sublattices of the kagome lattice remains predominantly unswitched, corresponding to magnetization $M/M_s = 1/2$. In this regime, nearly all monopoles have met their fate and end up pinned on a neighbouring string. The final stages of the hysteresis are characterized by a flipping of individual islands corresponding to the remaining sublattice. This regime involves the condensation of charge defects, resulting in a sharp rise in their density ν. Shortly before this condensation is complete, the remaining defects should be described relative to the final saturated state (Supplementary Fig. S2).

1D nature of avalanches

Our observed magnetization reversal by means of Dirac string formation is an entirely 1D process and therefore is in contrast to other 2D and 3D systems where magnetization reversal occurs by means of the nucleation and growth of domains that are extensive in system dimensions[36,37]. The latter processes are successfully described by the scaling theory of Sethna, Dahmen *et al.*[38,39] for the random field Ising model (RFIM) that predicts a power-law behaviour for the avalanche probability $P(s)$ as a function of the number s of spins participating in an avalanche. In our case, the probability $P(s)$ for the occurrence of a Dirac string avalanche decays exponentially with its length s, as shown in Fig. 4b. This exponential decay demonstrates that we are dealing with a fundamentally new type of avalanche behaviour, namely the propagation of a 1D avalanche in a 2D system, providing an example of dimensional reduction due to frustration[12]. In addition to being observed in numerical simulations of the 1D RFIM (ref. 40), such exponential behaviour can be understood by the

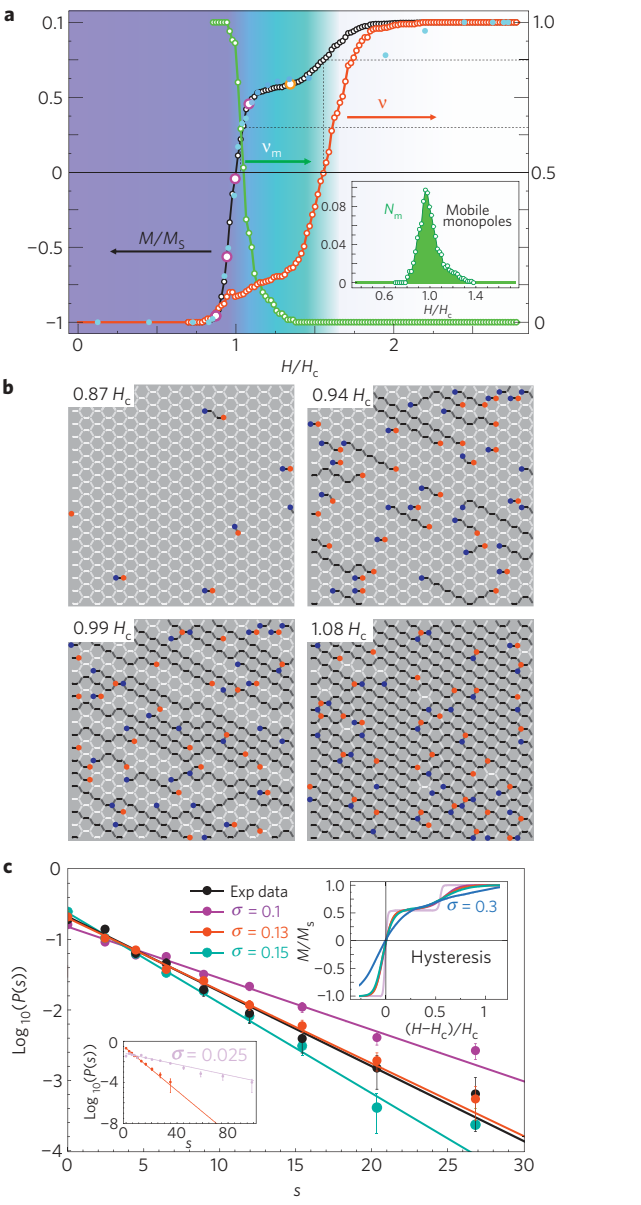

Figure 5 | Hysteresis, avalanches and disorder—Monte-Carlo simulations. Monte Carlo simulations based on a random switching field $H_S = H_0\xi$ with $\mu_0 H_0 = 12.3$ mT, and a dimensionless Gaussian random variable ξ with $\langle\xi\rangle = 1$ and standard deviation σ (see Methods). **a**, Hysteresis, charge defect density ν, and fraction of mobile monopoles ν_m as explained in Fig. 4 for $\sigma = 0.13$. Shown are the Monte Carlo results together with the experimental data (blue). In agreement with experiments, there exists a plateau at large fields that corresponds to a stripe phase of Dirac strings. Note that the dipolar interaction renormalizes the coercivity to a value of $\mu_0 H_c = 17.7$ mT and is consistent with the coercivity recorded with magneto optical Kerr effect measurements. **b**, Characteristic magnetization configurations corresponding to the field values in **a**, which are highlighted in purple (orange, see Supplementary Fig. S3). **c**, Disorder dependence of the avalanche statistics. The avalanche probability decays exponentially for a large range of disorder, including the experimentally unattainable small value of $\sigma = 0.025$ (see inset). Error bars are statistical, derived from the square root of the number of events. Note that the avalanche statistics is a much more sensitive measure of disorder than the shape of the hysteresis (see inset) and we obtain agreement with experimental data for $\sigma = 0.13$, as used in **a**. In addition, the plateau associated with stripe formation of Dirac strings entirely disappears for high disorder ($\sigma = 0.3$) when coherent avalanches no longer exist.

following heuristic argument: the probability $P(s)$ of forming an avalanche of length s from a pre-existing string is $P(s) \propto p^s(1-p)\Delta h$, where $\Delta h = \Delta H/H_c$ is the reduced field step, and p is the probability for the flipping of an island moment subject to the condition that one of its neighbours has flipped. Nucleation of a monopole–antimonopole pair and subsequent string growth leads to qualitatively similar behaviour, except for an additional factor $p_0 \ll p$ describing the initial nucleation probability of an isolated island. Similarly, modifications resulting from nucleation of two strings and their subsequent coalescence do not change this exponential behaviour, nor is it changed by the finite trapping probability of a monopole on a neighbouring string. We emphasize that these 1D avalanches occur here in a system that is characterized by well-isolated nanoislands with a finely tuned geometry. A related system[26] of an interconnected honeycomb network also shows monopole-type defects, although the MFM technique together with the interconnectivity does not allow the identification of Dirac strings, and the avalanche behaviour appears to be 2D in nature (see Supplementary Information of ref. 26).

Avalanche statistics and role of disorder

We have carried out Monte Carlo simulations to quantify the role of disorder in our system and to gain a more detailed insight into the dependence of the avalanche statistics on this disorder. The long-range dipolar interaction has been implemented using Ewald's method, with the strength of the interaction completely determined by the experimental parameters. The random switching field for a particular island is given by $H_S = H_0\xi$, where ξ is a dimensionless Gaussian random variable with $\langle\xi\rangle = 1$ and the disorder is characterized by $\sigma = (\langle(\xi - \langle\xi\rangle)^2\rangle)^{1/2}$. The resulting hysteresis loop with four representative magnetization configurations is shown in Fig. 5 for $\sigma = 0.13$ and $\mu_0 H_0 = 12.3$ mT. The agreement with experiment is excellent, not only for the magnetization but also for the corresponding configurations in Fig. 5b, the related density ν of charge defects, and the fraction ν_m of mobile monopoles. This confirms both the finely tuned nature of the experimental system and the adequacy of our model. A small difference in the size of the hysteresis plateau between experiment and simulation can partially be traced back to the fact that this region is found to be considerably sample dependent in the simulations. We emphasize that in the strongly coupled regime investigated here, both our observations and our simulations reveal that the avalanches propagate island-by-island, coherently transporting the monopoles along the path traced out by the Dirac string. This is in contrast to 'popping-noise' behaviour[39] at low coupling[41] or high disorder, where islands can flip randomly and independently of each other. This may fortuitously lead to the formation of short string-like defects, which are unrelated to the coherent Dirac string growth observed here.

Monte Carlo results of both avalanche statistics and hysteresis curves are shown in Fig. 5c for varying disorder, based on experimental values of the dipolar coupling. Note that the avalanche statistics is much more sensitive to disorder than the hysteresis and hence provides a more accurate measure of the disorder σ. The exponential decay of $P(s)$ persists to disorder values as small as $\sigma = 0.025$, which is five times smaller than the experimentally attainable value. Indeed, this latter value of disorder corresponds to $\sigma H_0/H_{dip} \ll 1$, a regime where a higher dimensional RFIM would have predicted a power-law dependence. This demonstrates again the 1D nature of our Dirac string avalanches and provides a striking example of dimensional reduction due to frustration[12].

Methods

Theory. The dipolar interaction between sites on the kagome lattice is given by

$$E_{dip} = \frac{\mu_0}{8\pi} \sum_{i,j(i\neq j)} \frac{1}{r_{ij}^3}[\mathbf{m}_i \cdot \mathbf{m}_j - 3(\mathbf{m}_i \cdot \hat{\mathbf{r}}_{ij})(\mathbf{m}_j \cdot \hat{\mathbf{r}}_{ij})]$$

where $\mathbf{m}_i = \tau_i m \mathbf{e}_i$ is the magnetic moment at site i. Here the pseudospin $\tau_i = \pm 1$ denotes the projection of the spin onto the anisotropy (local Ising) directions $\mathbf{e}_i$ (directed along the links of the honeycomb lattice, see Fig. 1), and $m = 1.1 \times 10^{-15}$ A m^2 is the magnetic moment of a permalloy island. Within the charge model[6], each dipole is replaced by a dumbbell of two opposite charges of magnitude $q = m/a_h$, which are situated at the neighbouring vertices of the honeycomb lattice, separated by a_h. Introducing the total charge at the vertex α of the honeycomb lattice, $Q_\alpha = \sum_{n\in\alpha} q_n$, the total energy takes the form of a magnetic analogue[6] of Coulomb's law, $(1/2)\sum_{\alpha,\beta} V(r_{\alpha\beta})$, where

$$V(r_{\alpha\beta}) = \begin{cases} \dfrac{\mu_0}{4\pi}\dfrac{Q_\alpha Q_\beta}{r_{\alpha\beta}}, & \alpha \neq \beta \\ v_0 Q_\alpha^2, & \alpha = \beta \end{cases}$$

Here the 'charging energy' coefficient v_0 results from the interaction of charges at the same site. If we take into account the realistic particle shape as shown in Fig. 1a, then this energy results from the interaction between charges that are situated at the semicircular ends of different permalloy islands around a vertex[34]. The ends are separated from the vertices of the honeycomb lattice by $d = 60$ nm and have the same radius. This leads to an interaction energy of $v_0 = 3.5/a_k$, where $a_k = 500$ nm is the nearest-neighbour distance of the kagome lattice. Note that higher order multipole contributions of this charge distribution to the energy are small[34], being of order $(2d/a_h)^2 \simeq 0.04$, and play a negligible role. Remarkably, a value of $v_0 = 3.56/a_k$ results when one adjusts the onsite repulsion to match the nearest-neighbour dipolar interaction (see Supplementary Information of ref. 6). Note that the non-observation of charge defects with $\Delta Q_\alpha = \pm 4q$ (see Fig. 2, column IV) can be explained by considering the charge model. Taking the example of a regime with a small charge defect density, where the moving monopoles do not encounter other Dirac strings, such an excitation would correspond to a configuration where the chain of reversed islands grows 'around a corner', that is, in the opposite direction to the original Dirac string propagation. Compared with the observed Dirac string propagation, the creation of a $\Delta Q = \pm 4q$ defect is energetically unfavourable as it would involve both a higher nearest-neighbour charge interaction energy and a smaller Zeeman energy gain.

Experiment. Quasi-infinite arrays (50 μm × 50 μm) of elongated permalloy (Ni80% Fe20%) nanomagnets were created with electron beam lithography in combination with d.c. magnetron sputtering and lift-off (Fig. 1a; ref. 28). The permalloy islands are 20 nm thick, the distance between the centres of two neighbouring islands $a_k = 500$ nm and the length and width of each island are 470 nm and 160 nm, respectively. Magnetic imaging was carried out with photoemission electron microscopy at the SIM beamline at the Swiss Light Source, Paul Scherrer Institute. Employing XMCD, the artificial kagome spin ice was imaged by tuning the X-ray energy to the Fe L_3-edge. Dividing two images, taken with left and right circular polarized light, leads to an XMCD image with increased magnetic contrast, where the intensity is a measure of the angle between the circular X-ray polarization vector and the magnetization[42]. Ferromagnetic islands with moments parallel or antiparallel to the X-ray polarization vector appear black or white in the XMCD image, respectively, whereas islands with moments at ±60° or ±120° to the polarization vector will have a dark grey or light grey contrast, respectively (see Fig. 1). For observations of the magnetization reversal, the samples were mounted in a magnetizing holder that allowed the *in situ* application of in-plane magnetic fields up to ±50 mT. As a result of the difficulties in obtaining an XMCD image in an applied field, which disturbs the low-energy electrons in the photoemission electron microscope, the observations were carried out at remanence, that is, XMCD images were recorded after reducing the applied field to zero. Correspondingly, the hysteresis is shown in the form of a remanence curve, that is, with the field switched off after each field step. The dimensionless smeared charge density shown in Fig. 3 is defined as $\tilde{\rho}_m = (\Delta x)^2 \rho_m/q$, where the smeared charge density ρ_m is the convolution of the total charge Q_α with a Gaussian of FWHM, $\Delta x = 2a_h$.

Simulations. Monte Carlo simulations have been carried out on a rectangular patch consisting of 1,020 islands. The islands are represented by dipoles located at the sites of the kagome lattice with an anisotropy forcing the magnetic moments to point along the island axis. Using Ewald's summation technique, the dipolar interaction has been summed over periodic replicas of the patch extending to infinity. The strength of the dipolar interaction is given by the parameters characterizing our experimental system. The random switching field of individual islands is given by $H_S = H_0\xi$, where ξ is a dimensionless Gaussian random variable with $\langle\xi\rangle = 1$ and $\sigma \equiv (\langle(\xi - \langle\xi\rangle)^2\rangle)^{1/2}$. Single-spin flips were accepted when the projection of the local fields along the island axis exceeded the random switching field H_S of a particular island. In our simulations, we verified that the string growth proceeds island-by-island in an avalanche-type fashion. The hysteresis loop was calculated by taking the configuration of the previous field as a starting configuration for the new field value. Horizontal islands contribute to the magnetization with weight 1 and diagonal ones with weight 1/2. The avalanche statistics per field step were averaged over 16 different 'samples', that is, 16 different realizations of the disorder. The avalanche statistics were accumulated over equal field steps within the steep rise of the hysteresis, with the slope of $\log_{10} P(s)$

independent of the field step size, following from the discussion of $P(s)$ in the main text. To obtain good agreement of the real-space images with the experimental data, the field was applied under a small angle $\pi/50$ in the negative y-direction, but the avalanche statistics were seen to be independent of this angle as long as it was kept small. For rare events, a binning procedure has been used, as described in ref. 43. Also note that the toroidal nature of the boundary conditions and the 1D nature of the avalanches allowed us to explore avalanche lengths exceeding the system size in the low disorder limit, as the avalanches can wrap around the sample several times.

Received 22 September 2009; accepted 18 August 2010; published online 17 October 2010

References

1. Dirac, P. A. M. Quantised singularities in the electromagnetic field. *Proc. R. Soc. Lond. A* **133,** 60–72 (1931).
2. 't Hooft, G. Magnetic monopoles in unified gauge theories. *Nucl. Phys. B* **79,** 276–284 (1974).
3. Polyakov, A. M. Particle spectrum in quantum field theory. *JETP Lett.* **20,** 194–195 (1974).
4. Goldhaber, A. S. & Trower, W. P. Magnetic monopoles. *Am. J. Phys.* **58,** 429–439 (1990).
5. Abbiendi, G. *et al.* Search for Dirac magnetic monopoles in e^+e^- collisions with the OPAL detector at LEP2. *Phys. Lett. B* **663,** 37–42 (2008).
6. Castelnovo, C., Moessner, R. & Sondhi, S. L. Magnetic monopoles in spin ice. *Nature* **451,** 42–45 (2008).
7. Harris, M. J., Bramwell, S. T., McMorrow, D. F., Zeiske, T. & Godfrey, K. W. Geometrical frustration in the ferromagnetic pyrochlore $Ho_2Ti_2O_7$. *Phys. Rev. Lett.* **79,** 2554–2557 (1997).
8. Bramwell, S. T. & Gingras, M. J. P. Spin ice state in frustrated magnetic pyrochlore materials. *Science* **294,** 1495–1501 (2001).
9. Ramirez, A. P., Hayashi, A., Cava, R. J., Siddharthan, R. & Shastry, B. S. Zero-point entropy in 'spin ice'. *Nature* **399,** 333–335 (1999).
10. Pauling, L. The structure and entropy of ice and of other crystals with some randomness of atomic arrangement. *J. Am. Chem. Soc.* **57,** 2680–2684 (1935).
11. Tchernyshyov, O. Magnetism: Freedom for the poles. *Nature* **451,** 22–23 (2008).
12. Balents, L. Spin liquids in frustrated magnets. *Nature* **464,** 199–208 (2010).
13. Heeger, A. J., Kivelson, S., Schrieffer, J. R. & Su, W. P. Solitons in conducting polymers. *Rev. Mod. Phys.* **60,** 781–850 (1988).
14. Faddeev, L. D. & Takhtajan, L. A. What is the spin of a spin-wave? *Phys. Lett. A* **85,** 375–377 (1981).
15. Lake, B., Tennant, D. A., Frost, C. D. & Nagler, S. E. Quantum criticality and universal scaling of a quantum antiferromagnet. *Nature Mat.* **4,** 329–334 (2005).
16. Braun, H. B. *et al.* Emergence of soliton chirality in a quantum antiferromagnet. *Nature Phys.* **1,** 159–163 (2005).
17. dePicciotto, R. *et al.* Direct observation of a fractional charge. *Nature* **389,** 162–164 (1997).
18. Dolev, M., Heiblum, M., Umansky, V., Stern, A. & Mahalu, D. Observation of a quarter of an electron charge at the $\nu = 5/2$ quantum Hall state. *Nature* **452,** 829–835 (2008).
19. Jaubert, L. D. C. & Holdsworth, P. C. W. Signature of magnetic monopole and Dirac string dynamics in spin ice. *Nature Phys.* **5,** 258–261 (2009).
20. Morris, D. J. P. *et al.* Dirac strings and magnetic monopoles in spin ice $Dy_2Ti_2O_7$. *Science* **326,** 411–414 (2009).
21. Fennell, T. *et al.* Magnetic Coulomb phase in the spin ice $Ho_2Ti_2O_7$. *Science* **326,** 415–417 (2009).
22. Bianchi, A. D. *et al.* Superconducting vortices in $CeCoIn_5$: Toward the Pauli-limiting field. *Science* **319,** 177–180 (2008).
23. Laver, M. & Forgan, E. M. Magnetic flux lines in type-II superconductors and the hairy ball theorem. *Nature Comm.* **1,** 1–4 (2010).
24. Nelson, D. R. *Defects and Geometry in Condensed Matter Physics* 303 (Cambridge Univ. Press, 2002).
25. Kadowaki, H. *et al.* Observation of magnetic monopoles in spin ice. *J. Phys. Soc. Jpn* **78,** 103706 (2009).
26. Ladak, S., Read, D. E., Perkins, G. K., Cohen, L. F. & Branford, W. R. Direct observation of magnetic monopole defects in an artificial spin-ice system. *Nature Phys.* **6,** 359–363 (2010).
27. Wang, R. F. *et al.* Artificial 'spin ice' in a geometrically frustrated lattice of nanoscale ferromagnetic islands. *Nature* **439,** 303–306 (2006).
28. Mengotti, E. *et al.* Building blocks of an artificial kagome spin ice: Photoemission electron microscopy of arrays of ferromagnetic islands. *Phys. Rev. B* **78,** 144402 (2008).
29. Remhof, A. *et al.* Magnetostatic interactions on a square lattice. *Phys. Rev. B* **77,** 134409 (2008).
30. Möller, G. & Moessner, R. Artificial square ice and related dipolar nanoarrays. *Phys. Rev. Lett.* **96,** 237202 (2006).
31. Wills, A. S., Ballou, R. & Lacroix, C. Model of localized highly frustrated ferromagnetism: The kagome spin ice. *Phys. Rev. B* **66,** 144407 (2002).
32. Tabata, Y. *et al.* Kagome ice state in the dipolar spin ice $Dy_2Ti_2O_7$. *Phys. Rev. Lett.* **97,** 257205 (2006).
33. Fennell, T., Bramwell, S. T., McMorrow, D. F., Manuel, P. & Wildes, A. R. Pinch points and Kasteleyn transitions in kagome ice. *Nature Phys.* **3,** 566–571 (2007).
34. Möller, G. & Moessner, R. Magnetic multipole analysis of kagome and artificial spin-ice dipolar arrays. *Phys. Rev. B* **80,** 140409 (2009).
35. Chern, G. W., Mellado, P. & Tchernyshyov, O. Two-stage ordering of spins in dipolar spin ice on kagome. Preprint at http://arxiv.org/abs/0906.4781 (2009).
36. Im, M. Y., Fischer, P., Kim, D. H. & Shin, S. C. Direct observation of individual Barkhausen avalanches in nucleation-mediated magnetization reversal processes. *Appl. Phys. Lett.* **95,** 182504 (2009).
37. Sethna, J. P. *et al.* Hysteresis and hierarchies: Dynamics of disorder-driven first-order phase transformations. *Phys. Rev. Lett.* **70,** 3347 (1993).
38. Sethna, J. P., Dahmen, K. A. & Myers, C. R. Crackling noise. *Nature* **410,** 242–250 (2001).
39. Sethna, J. P., Dahmen, K. A. & Perkovic, O. Random-field Ising models of hysteresis. Preprint at http://arxiv.org/abs/0406320 (2004).
40. Chubykalo, O. A., González, J. M. & González, J. Avalanches as propagating domain walls in a micromagnetic model. *Physica D* **113,** 382–386 (1998).
41. Schumann, A., Sothmann, B., Szary, P. & Zabel, H. Charge ordering of magnetic dipoles in artificial honeycomb patterns. *Appl. Phys. Lett.* **97,** 022509 (2010).
42. Stöhr, J. *et al.* Element-specific magnetic microscopy with circularly polarized X-rays. *Science* **259,** 658–661 (1993).
43. Christensen, K. & Moloney, N. R. *Complexity and Criticality* (Imperial College Press, 2005).

Acknowledgements

The authors would like to thank: M. Horisberger, E. Deckardt, A. Weber, C. David, A. Steger, L. Le Guyader, A. Kleibert, J. Raabe, D. Eastwood and D. Atkinson for their help. We also acknowledge helpful discussions with V. Lobaskin, W. Nahm and M. Sigrist. This work was supported by the Swiss National Science Foundation and the Science Foundation of Ireland (08/RFP/PHY1532 and 05/IN1/I853), and part of this work was carried out at the Swiss Light Source, Paul Scherrer Institute, Villigen, Switzerland. We also acknowledge receipt of an HEA Ireland equipment fund.

Author contributions

Sample preparation: E.M.; measurements: E.M., A.F.R.; analysis and interpretation: E.M., L.J.H., H.B.B.; theory and simulations: R.V.H., H.B.B.; preparation of the manuscript: E.M., L.J.H., H.B.B.; supervision of the project: L.J.H., H.B.B., F.N. All authors discussed the results and implications, and commented on the manuscript at all stages.

Additional information

The authors declare no competing financial interests. Supplementary information accompanies this paper on www.nature.com/naturephysics. Reprints and permissions information is available online at http://npg.nature.com/reprintsandpermissions. Correspondence and requests for materials should be addressed to L.J.H. or H.B.B.